Thiazolothiazole-Based Luminescent Metal–Organic Frameworks with Ligand-to-Ligand Energy Transfer and Hg^{2+} Sensing Capabilities

Amina Khatun,[1] Dillip K. Panda,[1] Nickolas Sayresmith,[2] Michael G. Walter,[2] and Sourav Saha[1,*]

[1]Department of Chemistry, Clemson University, 211 S. Palmetto Blvd, Clemson, South Carolina 29634, United States

[2]Department of Chemistry, University of North Carolina Charlotte, 9201 University Center Blvd, Charlotte, North Carolina 28228, United States

*Email: souravs@clemson.edu

ABSTRACT: Photoinduced electron and energy transfer through preorganized chromophore, donor, and acceptor arrays are key to light-harvesting capabilities of photosynthetic plants and bacteria. Mimicking the design principles of natural photosystems, we constructed a new luminescent pillared paddlewheel metal–organic framework (MOF), $Zn_2(NDC)_2(DPTTZ)$ featuring naphthalene dicarboxylate (NDC) struts that served as antenna chromophores and energy donors and *N,N′*-di(4-pyridyl)thiazolo-[5,4-d]thiazole (DPTTZ) pillars as complementary energy acceptors and light emitters. Highly ordered arrangement and good overlap between the emission and absorption spectra of these two complementary energy donor and acceptor units enabled ligand-to-ligand Förster resonance energy transfer, allowing the MOF to display exclusively DPTTZ-centric blue emission (410 nm) regardless of the excitation of either chromophore at different wavelengths. In the presence of Hg^{2+}, a toxic heavy metal ion, the photoluminescence (PL) of $Zn_2(NDC)_2(DPTTZ)$ MOF underwent significant red-shift to 450 nm followed by quenching, whereas other transition metal ions (Mn^{2+}, Fe^{2+}, Co^{2+}, Ni^{2+}, Cu^{2+} and Cd^{2+}) caused only fluorescence quenching but no shift. The free DPTTZ ligand also displayed similar, albeit less efficient, fluorescence changes, suggesting that the heavy atom effect and coordination of Hg^{2+} and other transition metal ions with the DPTTZ ligands were responsible for the fluorescence changes in the MOF. When exposed to a mixture of different metal ions including Hg^{2+}, the MOF still displayed the Hg^{2+}-specific fluorescence signal, demonstrating that it could detect Hg^{2+} in the presence of other metal ions. The powder x-ray diffraction studies verified that the framework remained intact after being exposed to Hg^{2+} and other transition metal ions, and its original PL spectrum was restored upon washing. These studies demonstrated the light-harvesting and Hg^{2+} sensing capabilities of a new bichromophoric luminescent MOF featuring a seldom-used photoactive ligand, which will likely spark an explosion of TTZ-based MOFs for various optoelectronic applications in near future.

KEYWORDS: *metal–organic frameworks, energy transfer, light-harvesting, luminescence, sensing*

INTRODUCTION

Photoinduced cascade electron transfer and energy transfer through preorganized chromophores and donor–acceptor arrays are key steps of light-harvesting mechanisms of photosynthetic plants and bacteria.[1] These well-orchestrated intricate events are not only the primary source of food and energy supplies that propel life on earth, but also offer scientists clues for how to design artificial light-harvesting materials that can power and advance human civilization in a sustainable way. The first and foremost criterion for efficient electron/energy transfer events is precise organization of chromophore, donor, and acceptor units with complementary energy levels so that the photons and/or electrons released by the former can be received by the latter.[2] Among various supramolecular and polymeric materials developed to date,[3–6] metal–organic frameworks (MOFs)[7]—a class of crystalline porous coordination networks composed of metal cluster nodes and organic linkers—present one of the most effective ways to organize these components in a highly ordered periodic fashion that can foster efficient energy and electron transfer processes when the requisite criteria are satisfied. Furthermore, tunable reticular structures, porosity and chemical and physical properties make MOFs one the most versatile materials that can not only capture and concentrate certain analytes selectively, but also exhibit stimuli-responsive behaviors upon specific host-guest interactions.[8] As a result, although much of MOF research in early days largely focused on their size- and shape-selective guest encapsulation, separation, storage, sequestration, and delivery applications,[9–15] the introduction of redox- and photoactive ligands,[15–17] metal ions,[18] and guest molecules[19–21] endowed them with fascinating optical, electronic, and chemical properties,[22,23] unlocking their potential for photocatalysis,[24,25] sensing[8,26–40] electrical[41–52] and ionic conductivities[53–61] and light-to-electrical energy conversion.[62–70]

Photoluminescence (PL) is one of the most appealing and useful properties of MOFs. While some frameworks display photoluminescence despite not containing intrinsically emissive components due to ligand rigidification,[8,27] the most effective and tunable luminescent MOFs usually feature luminescent aromatic ligands and lanthanide ions that emit light upon direct or indirect sensitization involving ligand-to-ligand or ligand-to-metal energy transfer events.[71] Although ligand-to-ligand energy transfer events are most commonly found in porphyrin-based MOFs,[72–78] porphyrins are rather weak fluorophores and very prone to photobleaching. Therefore, there remains a need for porphyrin-free luminescent MOFs that can support energy transfer and display stimuli-responsive emission changes. Diversifying the composition, properties, and functions of light-harvesting MOFs, herein, we report synthesis, PL behavior, and energy transfer and Hg^{2+} sensing capabilities of a new pillared-paddlewheel framework $Zn_2(NDC)_2(DPTTZ)$ featuring 2,6-naphthalele dicarboxylate (NDC) struts and *N,N′*-di(4-pyridyl)thiazolo-[5,4-d]thiazole (DPTTZ) pillars (Figure 1), which are excellent chromophores and fluorophores with complementary absorption and emission characteristics suitable for Förster resonance energy transfer (FRET).[79,80] Although the redox and light-harvesting properties of electron deficient and luminescent TTZ compounds are well documented in molecular environments,[81,82] they have been rarely incorporated in MOFs[83–85] and their PL and redox properties have yet to be explored inside crystalline frameworks. The lowest energy absorption peak of DPTTZ overlaps quite well with the emission peak of NDC, which enables ligand-to-ligand FRET and allows the MOF to display exclusively DPTTZ-centric blue emission (~410 nm) irrespective of the excitation wavelength. Control MOFs devoid of either NDC or DPTTZ ligand do not display such energy transfer capability. Furthermore, the PL spectrum of the DPTTZ-based MOF undergoes significant bathochromic shift and quenching in the presence of Hg^{2+} but not with other transition metal ions, making it a promising sensor for this toxic heavy metal ion.

EXPERIMENTAL SECTION

General Materials and Methods. Starting materials including NDC, 1,4-benzenedicarboxylic acid (1,4-BDC), 4,4'-bipyridine (BPY), dithiooxamide, 4-pyridinecarboxaldehyde, $Zn(NO_3)_2.6H_2O$, $Hg(OTf)_2$, $Mn(NO_3)_2$, $Fe(ClO_4)_2$, $Co(NO_3)_2$, $Ni(NO_3)_2$, $Cu(NO_3)_2$, $Cd(NO_3)_2$, and solvents (DMF, MeCN, EtOH, $CHCl_3$, chlorobenzene, etc.) were purchased from Sigma-Aldrich, Acros Organic, TCI America, and VWR and used as-obtained. The ^{1}H NMR spectra were recorded on a Bruker 500 MHz NMR spectrometer. Single crystal x-ray diffraction (SXRD) analyses of MOF crystals were performed on a Bruker D8 Venture dual source diffractometer with Cu and Mo radiation sources and CMOS detector and structures were solved and refined using Bruker SHELXTL software package. Powder x-ray diffraction (PXRD) analyses were done with a Rigaku Ultima IV X-ray diffractometer equipped with Cu Kα radiation source (λ = 1.5406 Å) and a CCD area detector. The porosity of MOFs was determined from CO_2 sorption isotherms recorded on a Quantachrome Autosorb iQ Gas Sorption Analyzer and their thermal stability from thermogravimetric analysis (TGA) and differential scanning calorimetry (DSC) measured with a TA instrument SDT Q600. The UV-Vis absorption spectra of ligands and MOFs were recorded on a Shimadzu UV-2600 spectrophotometer equipped with an integrated sphere (200–1400 nm) and steady-state excitation and emission spectra with a Shimadzu RF-6000 equipped with xenon lamp. Time-correlated single photon counting (TCSPC) measurements were conducted on a Jobin Yvon-Spex Fluorolog equipped with a 389 nm diode laser. The TCSPC fluorescence decay data were fit to double and triple exponential decays using Igor Pro 6.3 software and in-house developed fitting/graphing scripts.

Synthesis and Characterization of DPTTZ Ligand. DPTTZ ligand was synthesized following a reported protocol.[86] Briefly, a solution mixture of dithiooxamide (200 mg, 1.66 mmol) and 4-pyridinecarboxaldehyde (0.4 mL, 4.4 mmol) in anhydrous DMF (10 mL) was heated under reflux for 2.5 h. Upon cooling the reaction mixture to room temperature, yellow crystalline product precipitated out, which was collected by filtration, washed with H_2O and MeOH, and dried under air (311 mg, 63% yield). The ^{1}H NMR spectrum of the product was in good agreement with that of DPTTZ reported in literature.[84]

Syntheses and Characterization of MOFs. $Zn_2(NDC)_2(DPTTZ)$ MOF was synthesized under standard solvothermal reaction conditions used for pillared paddlewheel architectures.[87,88] First, DPTTZ (6.0 mg, 0.02 mmol) was dissolved in hot DMF (5 mL) and added to a freshly prepared solution of $Zn(NO_3)_2{\cdot}6H_2O$ (11.90 mg, 0.04 mmol) and NDC (8.73 mg, 0.04 mmol) in DMF (1.5 mL) in a screw capped vial. Then the resulting reaction mixture was placed inside an oven and heated at constant 80 °C for 2 days to obtain pale yellow colored rod-shaped crystals suitable for single-crystal X-ray diffraction (SXRD) analysis. These crystals were washed with fresh DMF and MeOH and dried under vacuum to obtain the bulk material (7.9 mg, 44% yield). The SXRD analysis (Table S1) of as-synthesized crystals revealed a triclinic unit cell and yielded a total of 49321 reflections to a maximum θ of 26.39° (0.80 Å resolution), of which 4257 were independent (average redundancy 11.586, completeness = 99.5%, R_{int} = 5.87%, R_{sig} = 2.55%) and 3889 (91.36%) were greater than $2\sigma(F^2)$. The final cell constants of $\underline{a}$ = 8.0961(13) Å, $\underline{b}$ = 10.5093(15) Å, $\underline{c}$ = 12.981(2) Å, α = 75.761(5)°, β = 77.486(6)°, γ = 88.858(5)°, volume = 1044.5(3) Å^3, were based upon the refinement of the XYZ-centroids of reflections above 20 σ(I). The calculated minimum and maximum transmission coefficients were 0.7910 and 0.9360. The structure was solved and refined using space group *P*-1, with Z = 1 for the formula unit $C_{44}H_{34}N_6O_{10}S_2Zn_2$. The final anisotropic full-matrix least-squares

refinement on F^2 with 335 variables converged at R1 = 3.50% for the observed data and wR2 = 8.62% for all data. The goodness-of-fit was 1.093. The largest peak in the final difference electron density synthesis was 0.671 $e^-/Å^3$ and the largest hole was –0.913 $e^-/Å^3$ with an RMS deviation of 0.082 $e^-/Å^3$. On the basis of the final model, the calculated density was 1.592 g/cm^3 and F(000), 512 e^-.

A solvothermal reaction of $Zn(NO_3)_2 \cdot 6H_2O$ (11.90 mg, 0.04 mmol), DPTTZ (6.0 mg, 0.02 mmol), and BDC (6.73 mg, 0.04 mmol) and in DMF (6.5 mL) under the same conditions (80 °C, 2 d) yielded needle-shaped pale yellow crystals (6.6 mg, 62 % yield) suitable for SXRD analysis. The SXRD analysis (Table S1) revealed an orthorhombic unit cell and yielded a total of 23443 reflections to a maximum θ of 22.00° (0.95 Å resolution), of which 6124 were independent (average redundancy 3.828, completeness = 99.5%, R_{int} = 8.34%, R_{sig} = 7.07%) and 4833 (78.92%) were greater than $2\sigma(F^2)$. The final cell constants of a = 34.566(2) Å, b = 17.1421(8) Å, c = 17.1901(10) Å, volume = 10185.7(10) $Å^3$, were based upon the refinement of the XYZ-centroids of reflections above 20 σ(I). The calculated minimum and maximum transmission coefficients were 0.8214 and 1.0000. The structure was solved and refined using space group *Iba*2, with Z = 8 for the formula unit $C_{47}H_{31}N_9O_9S_4Zn_2$.[84,85] The final anisotropic full-matrix least-squares refinement on F^2 with 641 variables converged at R1 = 4.40% for the observed data and wR2 = 8.87% for all data. The goodness-of-fit was 1.017. The largest peak in the final difference electron density synthesis was 0.921 $e^-/Å^3$ and the largest hole was -0.357 $e^-/Å^3$ with an RMS deviation of 0.071 $e^-/Å^3$. On the basis of the final model, the calculated density was 1.467 g/cm^3 and F(000), 4576 e^-.

Steady-State and Time-Resolved Fluorescence Studies. For steady-state fluorescence analysis, DMF and chlorobenzene solutions of NDC and DPTTZ ligands and suspensions of $Zn_2(NDC)_2(DPTTZ)$, $Zn_2(BDC)_2(DPTTZ)_2$, and $Zn_2(NDC)_2(BPY)$ MOFs were used. For time-correlated single photon counting (TCSPC) measurements, drop-cast films of NDC, BDC, and DPTTZ ligands and MOFs were prepared on Fisherbrand Plain Microscope Slides from corresponding chlorobenzene solutions or suspensions (2 mg/mL, 0.25 mL). The films were allowed to dry in open air for 0.5 h before the measurements.

Fluorescence Sensing Studies. For fluorescence titration studies, stock solutions of $Hg(OTf)_2$, $Mn(NO_3)_2$, $Fe(ClO_4)_2$, $Co(NO_3)_2$, $Ni(NO_3)_2$, $Cu(NO_3)_2$, and $Cd(NO_3)_2$ in DMF (6 mM) were added to MOF suspensions (0.1 mg/mL, 2 mL) and spectra were recorded at increasing salt concentrations (10–1000 μM).

RESULTS AND DISCUSSION

Design, Synthesis, and Characterization of MOFs. Despite having strong emission in dilute solutions, many organic fluorophores often exhibit diminished fluorescence at higher concentrations as well as in solid state due to self-quenching. On the other hand, in crystalline MOFs, fluorescent ligands can be positioned periodically at certain distances such that their photoluminescence is preserved and even augmented. Taking advantage of this unique structural feature of MOFs, we synthesized a pillared paddlewheel architecture $Zn_2(NDC)_2(DPTTZ) \cdot (DMF)_2$ (Figure 1a) using NDC struts as energy donors and DPTTZ pillars as energy acceptors via a simple solvothermal reaction (*vide supra*). SXRD analysis revealed that the resulting rod-shaped pale yellow crystals possessed triclinic unit cells with *P*-1 space group. The $Zn_2(COO)_4$ paddlewheel nodes formed by NDC struts are located in the *ab*-planes while the axially coordinated DPTTZ pillars are aligned along the *c*-axis. The diagonal distances between Zn_2 nodes in a given plane are 19.04 and 17.86 Å, and the distance between the Zn_2 nodes bridged by DPTTZ pillars is 16.92 Å, i.e., the fluorescent ligands are enough separated to avoid self-quenching.[8,70] Furthermore, the

large separation and orientation of electron rich NDC struts and electron deficient DPTTZ pillars prevent π-donor/acceptor charge transfer interactions, which could quench their photoluminescence.

Interestingly, under the same solvothermal conditions, the reaction of $Zn(NO_3)_2 \cdot 6H_2O$, 1,4-BDC, and DPTTZ yielded $Zn_2(1,4\text{-BDC})_2(DPTTZ)_2 \cdot (DMF)$ framework with orthorhombic unit cell and *Iba*2 space group (Figure 1b) instead of a typical cubic pillared-paddlewheel architecture. This framework is analogous to a previously reported[84,85] $[Zn(1,3\text{-BDC})(DPTTZ)]_n$ and featured a different type of Zn_2 nodes made of two distorted octahedral Zn-centers, each connected to one chelating and two bridging carboxylate groups in the equatorial plane and two axial DPTTZ ligands. The closest distance between two parallel π-stacked DPTTZ ligands was around 3.6–4 Å, i.e., within the range of π–π-interaction. The experimental PXRD patterns of both DPTTZ-based MOFs (Figures 1c and d) were consistent with the corresponding simulated patterns, confirming that they were indeed phase-pure materials and maintained their structural integrity and crystallinity upon activation.

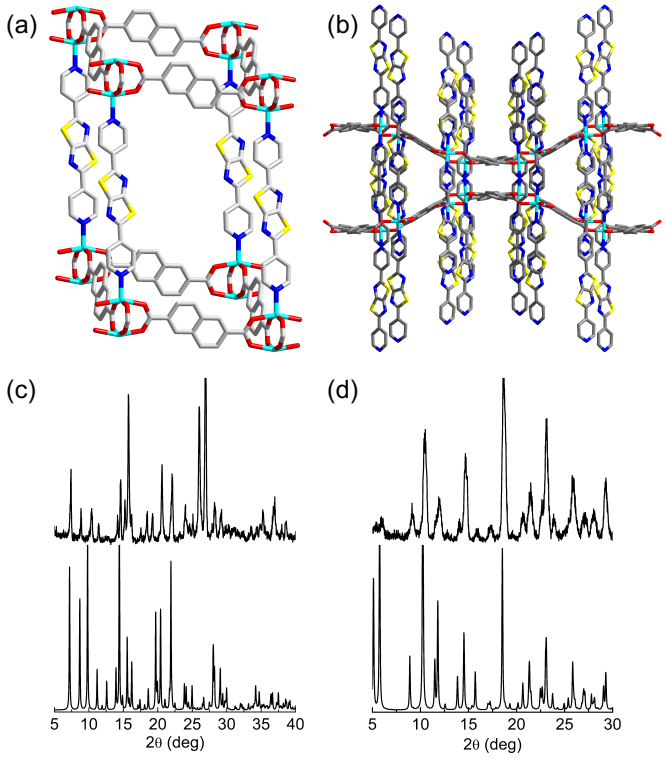

Figure 1. Single crystal structures of (a) $Zn_2(NDC)_2(DPTTZ)$ and (b) $Zn_2(1,4\text{-BDC})_2(DPTTZ)_2$ (cyan: Zn, blue: N, red: O, yellow: S, and grey: C). H atoms and disordered DMF molecules are omitted for clarity. The PXRD profiles of (c) $Zn_2(NDC)_2(DPTTZ)$ and (d) $Zn_2(1,4\text{-BDC})_2(DPTTZ)_2$ (bottom simulated, top experimental).

The thermogravimetric and differential scanning calorimetric analyses of $Zn_2(NDC)_2(DPTTZ)$ showed (Figure S1) that it lost only 5% of initial weight at 125–175 °C possibly due to the loss of residual DMF and remained stable up to 300 °C (30% weight loss). The TGA-DSC profiles of $Zn_2(1,4\text{-BDC})_2(DPTTZ)_2$

framework showed gradual weight loss (10%) between 130–230 °C and a significant drop above 330 °C, indicating it also has a reasonable thermal stability up to that temperature. Both frameworks displayed type-I CO_2-sorption isotherms (Figure S2), from which their Brunauer–Emmett–Teller (BET) surface areas and pore volumes were estimated. The surface area and pore volume of $Zn_2(NDC)_2(DPTTZ)$ are 106.8 m^2/g and 6.6 × 10^{-2} cm^3/g, respectively, and those for $Zn_2(1,4\text{-}BDC)_2(DPTTZ)_2$ are 113.4 m^2/g and 7.8 × 10^{-2} cm^3/g, respectively. Thus, both materials displayed comparable porosity despite having significant structural differences.

Steady-State and Time-Resolved Photoluminescence Properties of Ligands and MOFs. The excitation and emission spectra (Figure 2a) of NDC and DPTTZ ligands revealed excellent overlap between the emission peak of the former and the excitation (absorption) peak of the latter, which bodes well for ligand-to-ligand FRET. Upon excitation of NDC at 330 or 350 nm, it displayed an emission spectrum featuring two sharp peaks 360 and 375 nm and a prominent shoulder at ca. 400 nm, which overlapped quite well with the intense lowest energy excitation peak of DPTTZ at 390 nm responsible for $S_0 \rightarrow S_1$ transition. Upon its excitation at 390 nm, DPTTZ exhibits a strong emission peak at 410 nm. As a result, irrespective of the excitation wavelengths, a 1:1 NDC/DPTTZ solution mixture displayed (Figure S3) only DPTTZ-centric emission (410 nm) and none from NDC at a shorter wavelength, indicating that NDC struts acted as antenna chromophores.

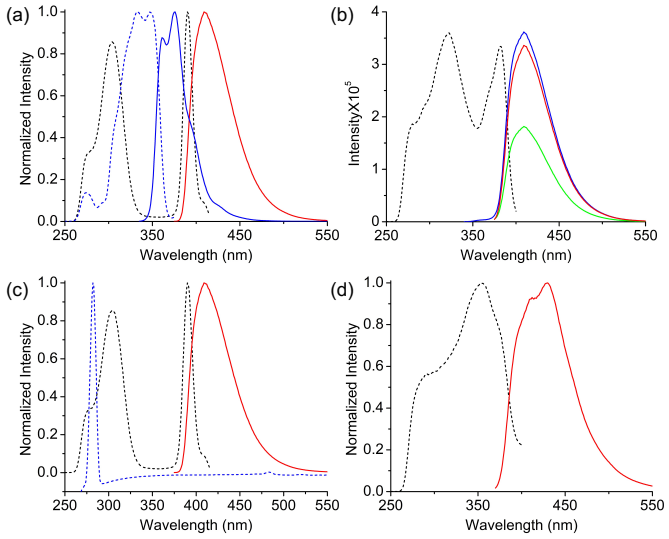

Figure 2. (a) The excitation (dashed lines) and emission (solid lines) spectra of free NDC (blue) and DPTTZ (red) ligands showing the requisite spectral overlap for FRET. (b) The excitation (dashed black line) and emission spectra of $Zn_2(NDC)_2(DPTTZ)$ showing exclusively DPTTZ-centric emission regardless of excitation wavelengths (λ_{Ex}: 320 (blue), 350 (green), and 380 nm (red)). (c) The excitation (dashed lines) and emission (solid lines) spectra of free BDC (blue) and DPTTZ (red) ligands showing the lack of spectral overlap required or FRET. (d) The excitation (dashed black line) and emission (solid red line) spectra of $Zn_2(1,4\text{-}BDC)_2(DPTTZ)_2$.

Encouraged by complementary absorption and emission characteristics of NDC and DPTTZ units, we turned our attention to PL properties of bichromophoric and control MOFs. Steady-state fluorescence studies of a $Zn_2(NDC)_2(DPTTZ)$ suspension in DMF revealed that (Figure 2b) irrespective of the excitation wavelengths, it only displayed the characteristic emission of DPTTZ at 410 nm and none from NDC struts, suggesting that the latter acted as antenna chromophores. As a result, exclusively DPTTZ-centric MOF emission (410 nm) was observed through both direct (380 nm) and indirect (320 nm) excitation.

In contrast, 1,4-BDC and DPTTZ did not share overlapping emission with absorption spectra, which eliminated the possibility of ligand-to-ligand energy transfer in the control MOF (Figure 2c). Therefore, $Zn_2(1,4\text{-}BDC)_2(DPTTZ)_2$ required direct excitation of DPTTZ ligands to display photoluminescence, which appeared at a slightly longer wavelength (435 nm) compared to that of $Zn_2(NDC)_2(DPTTZ)$ possibly because of π–π-interaction between the closely spaced (< 3.6–4 Å apart) parallel DPTTZ ligands (Figure 2d). Likewise, another control MOF $Zn_2(NDC)_2(BPY)$ devoid of energy accepting DPTTZ pillars only displayed a characteristic NDC emission peak at ca. 380 nm. The drop-cast MOF films displayed slightly longer wavelength emissions compared to respective suspensions (Figure S4).

Table 1: The fluorescence lifetimes (τ_F), quantum yields (Φ_F), radiative rates (k_F) of control and DPTTZ-based MOFs.

	τ_F (ps)	τ_F (ps)	Φ_F	k_F (s^{-1})
	suspension	**drop-cast film**	**suspension**	**suspension**
DPTTZ[80]	1044	461	0.22	2.11×10^8
$Zn_2(BDC)_2(DPTTZ)_2$	1077	953	0.27	2.50×10^8
$Zn_2(NDC)_2(DPTTZ)$	1006	620	0.38	3.78×10^8
$Zn_2(NDC)_2(BPY)$[88]	3393	1368		
$Zn_2(BDC)_2(BPY)$[88]	1235	470		

The fluorescence quantum yields (Φ_F) were obtained from steady-state fluorescence measurements. The TCSPC data (Figure 3) were fit into double and triple exponential decays to obtain fluorescence lifetimes (τ_F) and radiative decay rates (k_F) (Table 1). In general, the fluorescence lifetimes of MOFs measured in chlorobenzene suspensions were longer than in drop-cast films, which could be attributed to exciton-exciton interactions leading to fluorescence quenching in the films. However, thin-film measurements allowed for direct and more accurate comparisons between these MOFs and free fluorescent ligands. The fluorescence lifetime of DPTTZ (τ_F = 461 ps) became significantly longer when it was incorporated into MOFs: 953 ps in $Zn_2(1,4\text{-}BDC)_2(DPTTZ)_2$ and 620 ps in $Zn_2(NDC)_2(DPTTZ)$. The longer fluorescence lifetimes of the MOF-bound preorganized DPTTZ ligands can be attributed to diminished π–π-interaction between them, which could quench emission of aromatic fluorophores. The differences between fluorescence lifetimes of

dilute DPTTZ solution and DPTTZ-based MOF suspensions were less pronounced than in films (Table 1), as they all experienced longer lifetimes (~1 ns). Nevertheless, the fluorescence lifetimes of $Zn_2(NDC)_2(DPTTZ)$ containing complementary energy donor and acceptor ligands was shorter than that of $Zn_2(1,4\text{-}BDC)_2(DPTTZ)_2$ both in suspensions and thin-films, suggesting that singlet exciton delocalization was perhaps more effective in the former and singlet energy transfer was less efficient in the latter due to poor emission of BDC and the lack of overlap between BDC and DPTTZ emission and absorption spectra, respectively. The fluorescence quantum yields and radiative rates of DPTTZ increased slightly when it was incorporated into MOFs, which could be attributed to its rigidification and coordination with Lewis acidic Zn(II) centers. The alkylation of pyridyl groups of DPTTZ is also known to enhance its fluorescence.[80]

NDC has a fairly long fluorescence lifetime and rich photophysics in the long-UV region,[89] whereas BPY has very limited excitation and emission dynamics. Therefore, the photophysics of control MOF $Zn_2(NDC)_2(BPY)$ was dominated by NDC struts and showed extended fluorescent lifetimes: 1368 ps in drop-cast films and 3393 ps in suspension (Figure 3a). In comparison, the PL decay profile (Figure 3a) of $Zn_2(NDC)_2(DPTTZ)$ framework featuring complementary energy donor and acceptor units revealed significantly shorter fluorescence lifetimes both in thin-films (620 ps) and suspension (1006 ps), which were more comparable to that of DPTTZ than NDC. The excitation spectrum of this bichromophoric MOF indicated that NDC and DPTTZ ligands could be sensitized independently, however, its steady-state emission stemmed exclusively from the latter (Figure 2c) regardless of the excitation wavelength. Furthermore, the relative intensities of the DPTTZ-centric PL of the MOF upon indirect (NDC at 320 nm) and direct (DPTTZ at 380 nm) excitations were comparable. Together, these results indicated ^{1}*NDC to DPTTZ singlet energy transfer within this bichromophoric MOF. On the other hand, the PL lifetimes and decay profiles (Figure 3b) of $Zn_2(1,4\text{-}BDC)_2(DPTTZ)_2$ were comparable to that of $Zn_2(1,4\text{-}BDC)_2(BPY)$, indicating that there was no ligand-to-ligand energy transfer in either case, and the photophysics of the former was again dominated by DPTTZ ligands.

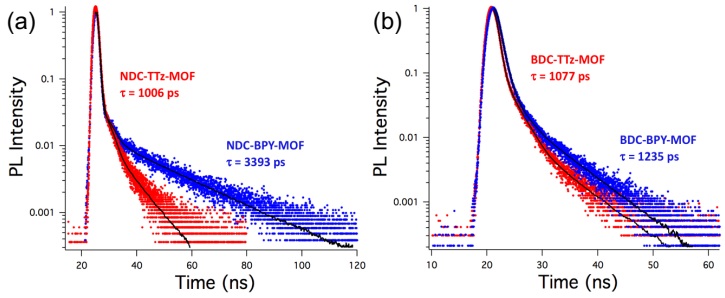

Figure 3. The comparisons between PL decay profiles of (a) $Zn_2(NDC)_2(DPTTZ)$ (red) and $Zn_2(NDC)_2(BPY)$ (blue) and (b) $Zn_2(1,4\text{-}BDC)_2(DPTTZ)_2$ and $Zn_2(1,4\text{-}BDC)_2(BPY)$ suspensions in chlorobenzene.

Hg^{2+} Ion Sensing with $Zn_2(NDC)_2(DPTTZ)$. Finally, we investigated the PL changes of $Zn_2(NDC)_2(DPTTZ)$ MOF in response to Hg^{2+}, a toxic heavy metal ion.[90–92] In the presence of a dilute $Hg(OTf)_2$ solution with concentration as low as 75 μM or 15 ppm, the emission peak of $Zn_2(NDC)_2(DPTTZ)$ suspension (0.1 mg/mL in DMF) (Figure 4a) started to shift to a longer wavelength

(450 nm) and its intensity also diminished. These changes could be attributed to heavy atom effect and possible coordination of Hg^{2+} with the sulfur atoms of DPTTZ ligands. This hypothesis was supported by the fact that in the presence of Hg^{2+}, free DPTTZ ligand also displayed similar PL quenching and bathochromic shift, whereas free NDC ligand exhibited only fluorescence quenching but no shift (Figure S5). Furthermore, despite Hg^{2+}-induced red-shift and partial quenching of $Zn_2(NDC)_2(DPTTZ)$ MOF fluorescence, the longest wavelength excitation peak (390 nm) associated with DPTTZ excitation remained unchanged, verifying that the new emission peak stemmed from DPTTZ-Hg^{2+} interactions. While both $Zn_2(NDC)_2(DPTTZ)$ MOF and free DPTTZ ligand displayed similar Hg^{2+}-induced PL changes, under the same conditions the PL quenching of the former was more significant (Figure S6), demonstrating that the DPTTZ-based MOF was more sensitive to Hg^{2+} than the free ligand. Upon washing the Hg^{2+}-treated $Zn_2(NDC)_2(DPTTZ)$ MOF with a copious amount of DMF, the new 450 nm emission peak disappeared and the original 410 nm peak reemerged (Figure 4b), demonstrating that the interaction of the MOF with Hg^{2+} and the corresponding PL changes were easily reversible. The Hg^{2+}-induced red-shift of $Zn_2(NDC)_2(DPTTZ)$ MOF photoluminescence was also visible in naked eye from the fluorescence microscope images of corresponding drop-cast films. The pristine MOF crystals displayed blue emission, whereas the Hg^{2+}-treated MOF appeared teal under the same irradiation (Figure 4b, inset).

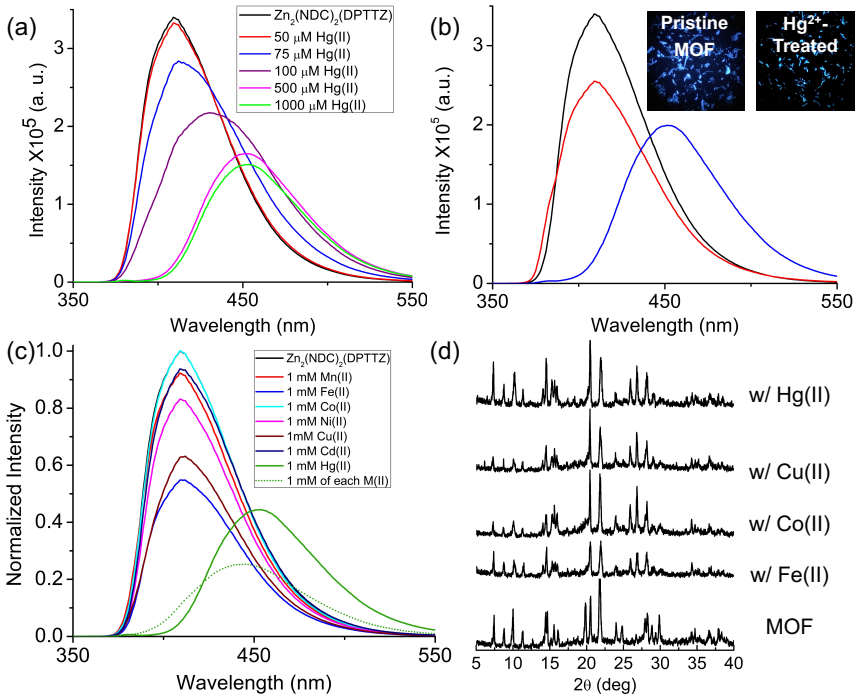

Figure 4. The PL response of $Zn_2(NDC)_2(DPTTZ)$ suspension (0.1 mg/mL in DMF) to (a) increasing concentration of $Hg(OTf)_2$ (50–1000 μM). (b) The PL spectra of pristine (black) and Hg^{2+}-treated $Zn_2(NDC)_2(DPTTZ)$ before (blue) and after (red) washing with DMF showing its reversible Hg^{2+} sensing capability. Inset: The fluorescence microscope images of pristine (left) and Hg^{2+}-treated (right) $Zn_2(NDC)_2(DPTTZ)$. (c) The PL changes of $Zn_2(NDC)_2(DPTTZ)$ in response to different transition metal ions individually (1 mM, color-coded solid lines) and as a mixture containing Hg^{2+} (1 mM each, dotted green line). (d) The PXRD profiles of $Zn_2(NDC)_2(DPTTZ)$ before and after being exposed to different metal ion solutions (1 mM in DMF) showing the stability of the framework.

Unlike Hg^{2+}, however, other transition metal ions, such as Mn^{2+}, Fe^{2+}, Co^{2+}, Ni^{2+}, Cu^{2+}, and Cd^{2+} did not cause any red-shift of $Zn_2(NDC)_2(DPTTZ)$ photoluminescence, and only Fe^{2+} and Cu^{2+} engendered significant fluorescence quenching (Figure 4c). The free DPTTZ ligand also displayed similar PL response to these metal ions (Figure S6), confirming that this ligand was indeed responsible for the cation-induced PL changes in the MOF. Thus, the Hg^{2+}-induced PL response of the MOF was unique, which bodes well for its sensing application. When exposed to a mixture of different metal ions including Hg^{2+}, the MOF still displayed the characteristic Hg^{2+}-specific PL signal (Figure 4c), i.e., it was able to detect Hg^{2+} in the presence of other metal ions. Furthermore, the PXRD profiles of $Zn_2(NDC)_2(DPTTZ)$ after being exposed to Hg^{2+} and other metal ions remained unchanged (Figure 4d), confirming that the framework retained its structural integrity under these conditions.

The strong similarities between the Hg^{2+}-induced PL changes of $Zn_2(NDC)_2(DPTTZ)$ MOF and free DPTTZ ligand, coupled with the reversibility of PL changes upon washing the MOF with pure solvents not only confirmed that the Hg^{2+}/DPTTZ interaction was responsible for the PL changes, but also ruled out a remote possibility of such changes being caused by metal ion exchange in $Zn_2(COO)_4$ paddlewheel nodes, which is a very slow process and unlikely to occur during the course of fairly quick (minutes) fluorescence titration experiments.[93] The PL changes of $Zn_2(NDC)_2(DPTTZ)$ MOF occurred at as low as 15 ppm of Hg^{2+} concentration, however, the amount of Hg^{2+} adsorbed by the MOF has not been determined by batch experiments. Nevertheless, the distinct and reversible Hg^{2+}-induced PL response rendered $Zn_2(NDC)_2(DPTTZ)$ MOF a promising Hg^{2+} sensor (in the tested organic solvent), although quantification of adsorbed Hg^{2+} remains to be done to fulfil all the necessary criteria of practical luminescent sensors.[40] It is worth noting that although several MOFs are known to display Hg^{2+}-induced fluorescence intensity changes,[32,33] unlike $Zn_2(NDC)_2(DPTTZ)$, they rarely exhibit totally new emission peaks in the presence of Hg^{2+}. Therefore, the Hg^{2+}-specific fluorescent changes of $Zn_2(NDC)_2(DPTTZ)$, which were distinct from that caused by other transition metal ions, made it more specific to Hg^{2+} and less susceptible to interference from other cations. Furthermore, owing to distinct excitation wavelengths of NDC and DPTTZ ligands and ligand-to-ligand energy transfer event, $Zn_2(NDC)_2(DPTTZ)$ can be sensitized at a wide wavelength region (275–400 nm) to access its blue photoluminescence and Hg^{2+} sensing capability, a scope that monochromophoric MOFs lack.

CONCLUSIONS

In summary, we have constructed a new luminescent pillared paddlewheel framework $Zn_2(NDC)_2(DPTTZ)$ featuring NDC struts as antenna chromophores and DPTTZ pillars as energy acceptors and light emitters. The overlapping emission and excitation spectra of these two ligands enabled efficient inter-ligand energy transfer leading to exclusively DPTTZ-centric emission regardless of the excitation wavelength, a phenomenon that is rarely seen outside porphyrin-based bichromophoric MOFs. The time-resolved fluorescence measurements revealed a much shorter excited state lifetime for $Zn_2(NDC)_2(DPTTZ)$ than control MOFs devoid of complementary energy donor and acceptor units. Furthermore, $Zn_2(NDC)_2(DPTTZ)$ was able to selectively sense Hg^{2+}, a toxic heavy metal ion, at ppm level. In the presence of Hg^{2+}, the characteristic DPTTZ-centric emission peak of this MOF underwent significant bathochromic-shift and quenching, while other transition metal ions caused only modest PL quenching but no shift. The PXRD profile of the Hg^{2+}-treated framework remained unchanged and the original PL

characteristic could be recovered by simply washing it with pure solvent, demonstrating that it could, in principle, serve as a reusable Hg^{2+} sensor. Although the limited hydrolytic stability of Zn-based MOFs could hinder real-life application of $Zn_2(NDC)_2(DPTTZ)$ as a practical Hg^{2+} sensor, this promising proof-of-concept demonstration inspired us to construct a TTZ-based Zr(IV) framework, which is expected to be water-stable at a wide pH range[32] and could qualify as a practical Hg^{2+} sensor. This work presents a new luminescent MOF based on a new fluorescent ligand with ligand-to-ligand energy transfer and selective Hg^{2+} sensing capabilities, which will likely spark a flurry of TTZ-based MOFs for various optoelectronic and sensing applications.

ASSOCIATED CONTENT

Supporting Information

The Supporting Information is available free of charge on the ACS Publications website at DOI: X. Additional crystallographic data, CIFs, CheckCIF, gas sorption isotherms, TGA, and PL data (PDF).

Accession Codes

CCDC 1916577 and 1916579 contain supplementary crystallographic data, which can be obtained free of charge via www.ccdc.cam.ac.uk/data_request/cif, or by emailing data_request@ccdc.cam.ac.uk, or by contacting The Cambridge Crystallographic Data Centre, 12 Union Road, Cambridge CB2 1EZ, UK; fax: +44 1223 336033.

AUTHOR INFORMATION

*Corresponding Author

Email: souravs@clemson.edu

ORCID

Sourav Saha: 0000-0001-6610-4820

Note

The authors declare no competing financial interest.

ACKNOWLEDGEMENTS

This work was supported by the National Science Foundation (award no. DMR-1809092) and Clemson University. We gratefully acknowledge Collin McMillen for assistance with crystal structure determination.

REFERENCES

1. Barber, J.; Andersson, B. Revealing the blueprint of photosynthesis. *Nature* **1994,** *370,* 31–34.
2. Valeur, B.; Berberan-Santos, M. Excitation Energy Transfer in *Molecular Fluorescence: Principles and Applications, 2nd ed*. Weinheim: Wiley-VCH. **2012,** 213–261.

3. Webber, S. E. Photon-harvesting polymers. *Chem. Rev.* **1990,** *90,* 1469–1482.
4. Aratani, N.; Kim, D.; Osuka, A. Discrete Cyclic Porphyrin Arrays as Artificial Light-Harvesting Antenna. *Acc. Chem. Res.* **2009,** *42,* 1922–1934.
5. Li, X.; Sinks, L. E.; Rybtchinski, B.; Wasielewski, M. R. Ultrafast Aggregate-to-Aggregate Energy Transfer within Self-assembled Light-Harvesting Columns of Zinc Phthalocyanine Tetrakis(Perylenediimide). *J. Am. Chem. Soc.* **2004,** *126,* 10810–10811.
6. Patwardhan, S.; Sengupta, S.; Siebbles, L. D. A.; Würthner, F.; Grozema, F. C. Efficient Charge Transport in Semisynthetic Zinc Chlorin Dye Assemblies. *J. Am. Chem. Soc.* **2012,** *134,* 16147–16150.
7. Furukawa, H.; Cordova, K. E.; O'Keeffe, M.; Yaghi, O. M. The Chemistry and Applications of Metal-Organic Frameworks. *Science* **2013,** *341,* 974–986.
8. Kreno, L. E.; Leong, K.; Farha, O. K.; Allendorf, M.; Duyne, R. P. V.; Hupp, J. T. Metal–Organic Framework Materials as Chemical Sensors. *Chem. Rev.* **2012,** *112,* 1105–1125.
9. Li, B.; Chrzanowski, M.; Zhang, Y.; Ma, S. Applications of Metal-Organic Frameworks Featuring Multi-Functional Sites. *Coord. Chem. Rev.* **2016,** *307,* 106–129.
10. He, Y.; Zhou, W.; Qian, G.; Chen, B. Methane storage in metal–organic frameworks. *Chem. Soc. Rev.* **2014,** *43,* 5657–5678.
11. Sumida, K.; Rogow, D. L.; Mason, J. A.; McDonald, T. M.; Bloch, E. D.; Herm, Z. R.; Bae, T.-H.; Long, J. R. Carbon Dioxide Capture in Metal–Organic Frameworks. *Chem. Rev.* **2012,** *112,* 724–781.
12. Li, J.-R.; Sculley, J.; Zhou, H.-C. Metal–Organic Frameworks for Separations. *Chem. Rev.* **2012,** *112,* 869–932.
13. Getman, R. B.; Bae, Y.-S.; Wilmer, C. E.; Snurr, R. Q. Review and Analysis of Molecular Simulations of Methane, Hydrogen, and Acetylene Storage in Metal–Organic Frameworks. *Chem. Rev.* **2012,** *112,* 703–723.
14. Huxford, R. C.; Rocca, J. D.; Lin, W. Metal–organic frameworks as potential drug carriers. *Curr. Opin. Chem. Biol.* **2010,** *14,* 262–268.
15. Chen, T.-H.; Popov, I.; Kaveevivitchai, W.; Miljanic, O. S. Metal−Organic Frameworks: Rise of the Ligands. *Chem. Mater.* **2014,** *26,* 4322–4325.
16. Paz, F. A. A.; Klinowski, J.; Viela, S. M. F.; Tomé, J. P. C.; Cavaleiro, J. A. S.; Rocha, J. Ligand design for functional metal–organic frameworks. *Chem. Soc. Rev.* **2012,** *41,* 1088–1110.
17. Lu, W.; Wei, Z.; Gu, Z.-Y.; Liu, T.-F.; Park, J.; Tian, J.; Zhang, M.; Zhang, Q.; Gentle III, T.; Bosch, M.; Zhou, H.-C. Tuning structure and function of metal–organic frameworks via linker design. *Chem. Soc. Rev.* **2014,** *43,* 5561–5593.
18. Gandara, F.; Uribe-Romo, F. J.; Britt, D. K.; Furukawa, H.; Lei, L.; Cheng, R.; Duan, X.; O'Keeffe, M.; Yaghi, O. M. Porous, Conductive Metal-Triazolates and Their Structural Elucidation by the Charge-Flipping Method. *Chem. Eur. J.* **2012,** *18,* 10595–10601.
19. Ullman, A. M.; Brown, J. W.; Foster, M. E.; Léonard, F.; Leong, K.; Stavila, V.; Allendorf, M. D. Transforming MOFs for Energy Applications Using Guest@MOF Concept. *Inorg. Chem.* **2016,** *55,* 7233–7249.
20. Allendorf, M.; Medishetty, R.; Fischer, R. A. Guest Molecule as a Design Element for Metal-Organic Frameworks. *MRS Bull.* **2016,** *41,* 865–869.

21. Allendorf, M. A.; Foster, M. E.; Léonard, F.; Stavila, V.; Feng, P. L.; Doty, F. P.; Leong, K.; Ma, E. Y.; Johnston, S. R.; Talin, A. A., Guest-Induced Emergent Properties in Metal−Organic Frameworks. *J. Phys. Chem. Lett.* **2015,** *6,* 1182–1195.
22. D'Alessandro, D. M. Exploiting redox activity in metal–organic frameworks: concepts, trends and perspectives. *Chem. Commun.* **2016,** *52,* 8957–8971.
23. Dolgopolova, E. A.; Shustova, N. B. Metal-Organic Frameworks Photophysics: Optoelectronic Devices, Photoswitches, Sensor, and Phtocatalysts. *MRS Bull.* **2016,** *41,* 890–896.
24. Zhang, T.; Lin, W. Metal–organic frameworks for artificial photosynthesis and photocatalysis. *Chem. Soc. Rev.* **2014,** *43,* 5982–5993.
25. Fateeva, A.; Chater, P. A.; Ireland, C. P.; Tahir, A. A.; Khimyak, Y. Z.; Wiper, P. V.; Darwent, J. R.; Rosseinsky, M. J. A Water-Stable Porphyrin-Based Metal–Organic Framework Active for Visible-Light Photocatalysis. *Angew. Chem. Int. Ed*. **2012,** *51,* 7440–7444.
26. Stassen, I.; Burtch, N.; Talin, A.; Falcaro, P.; Allendorf, M.; Ameloot, R. An updated roadmap for the integration of metal–organic frameworks with electronic devices and chemical sensors. *Chem. Soc. Rev.* **2017,** *46,* 3185–3241.
27. Hu, Z.; Deibert, B. J.; Li, J. Luminescent metal-organic frameworks for chemical sensing and explosive detection. *Chem. Soc. Rev.* **2014,** *43,* 5815–5840.
28. Nagarkar, S. S.; Joarder, B.; Chaudhari, A. K.; Mukherjee, S.; Ghosh, S. K. Highly Selective Detection of Nitro Explosives by a Luminescent Metal-Organic Framework. *Angew. Chem. Int. Ed.* **2013,** *52,* 2881–2885.
29. Hu, Z.; Lustig, W. P.; Zhang, J.; Zheng, C.; Wang, H.; Teat, S. J.; Gong, Q.; Rudd, N. D.; Li, J. Effective Detection of Mycotoxins by a Highly Luminescent Metal-Organic Framework. *J. Am. Chem. Soc.* **2015,** *137,* 16209–16215.
30. Shustova, N.B.; Cozzolino, A. F.; Reineke, S.; Baldo, M.; and Dinca, M. Selective Turn-On Ammonia Sensing Enabled by High-Temperature Fluorescence in Metal−Organic Frameworks with Open Metal Site. *J. Am.Chem. Soc.* **2013,** *135,* 13326–13329.
31. Shahat, A.; Hassan, H. M.; Azzazy, H. M. Optical Metal-Organic Framework Sensor for Selective Discrimination of Some Toxic Metal Ions in Water. *Anal. Chim. Acta* **2013,** *793,* 90–98.
32. Yee, K.-K.; Reimer, N.; Liu, J.; Cheng, S.-Y.; Yiu, S.-M.; Weber, J.; Stock, N.; Xu, Z. Effective Mercury Sorption by Thiol-Laced Metal−Organic Frameworks: in Strong Acid and the Vapor Phase. *J. Am. Chem. Soc.* **2013,** *135,* 7795–7798.
33. Liu, B.; Huang, Y.; Zhu, X.; Hao, Y.; Ding, Y.; Wei, W.; Wang, Q.; Qu, P.; Xu, M. Smart Lanthanide Coordination Polymer Fluorescence Probe for Mercury(II) Determination. *Anal. Chim. Acta* **2016,** *912,* 139–145.
34. Wu, L.-L.; Wang, Z.; Zhao, S.-N.; Meng, X.; Song, X.-Z.; Feng, J.; Song, S.-Y.; Zhang, H.-J. A Metal-Organic Framework/DNA Hybrid System as a Novel Fluorescent Biosensor for Mercury(II) Ion Detection. *Chem. Eur. J.* **2016,** *22,* 477–480.
35. Li, L.; Chen, Q.; Niu, Z.; Zhou, X.; Yang, T.; Huang, W. Lanthanide MOFs Assembled from Fluorene-Based Ligand: Selective Sensing of Pb^{2+} and Fe^{3+} Ions. *J. Mater. Chem. C* **2016,** *4,* 1900–1905.
36. Wang, H. M.; Yang, Y. Y.; Zeng, C. H.; Chu, T. S.; Zhu, Y. M.; Ng, S. W. A Highly Luminescent Terbium-Organic Framework for Reversible Detection of Mercury Ions in Aqueous Solution. *Photochem. Photobiol. Sci.* **2013,** *12,* 1700–1706.

37. Zhu, Y.-M.; Zeng, C.-H.; Chu, T.-S.; Wang, H.-M.; Yang, Y.-Y.; Tong, Y.-X.; Su, C.-Y.; Wong, W.-T. A Novel Highly Luminescent LnMOF Film: A Convenient Sensor for Hg^{2+} Detecting. *J. Mater. Chem. A* **2013,** *1,* 11312–11319.
38. Xu, H.; Gao, J.; Qian, X.; Wang, J.; He, H.; Cui, Y.; Yang, Y.; Wang, Z.; Qian, G. Metal−Organic Framework Nanosheets for Fast-Response and Highly Sensitive Luminescent Sensing of Fe^{3+}. *J. Mater. Chem. A* **2016,** *4,* 10900–10905.
39. Li, Q.; Wang, C.; Tan, H.; Tang, G.; Gao, J.; Chen, C.-H. A turn on fluorescent sensor based on lanthanide coordination polymer nanoparticles for the detection of mercury(II) in biological fluids. *RSC Adv.* **2016,** *6,* 17811–17817.
40. Daimantis, S. A.; Margariti, A.; Pournara, A.; D.; Papaefstathiou, G. S.; Manos, M. J.; Lazarides, T. Luminescent metal–organic frameworks as chemical sensors: common pitfalls and proposed best practices. *Inorg. Chem. Front.* **2018**, *5*, 1493–1511.
41. Sun, L.; Campbell, M. G.; Dincă, M. Electrically Conductive Porous Metal–Organic Frameworks. *Angew. Chem. Int. Ed*. **2016,** *55,* 3566–3579.
42. Stavila, V.; Talin, A. A.; Allendorf, M. D. MOF-based electronic and optoelectronic devices. *Chem. Soc. Rev.* **2014,** *43,* 5994–6010.
43. Givaja, G.; Amo-Ochoa, P.; Gomez Garcia, J. G.; Zamora, F. Electrical conductive coordination polymers. *Chem. Soc. Rev.* **2012,** *41,* 115–147.
44. Allendorf, M. D.; Schwartzberg, A.; Stavila, V.; Talin, A. A. A roadmap to implementing metal–organic frameworks in electronic devices: challenges and critical directions. *Chem. Eur. J.* **2011,** *17,* 11372–11388.
45. Park, S. S.; Hontz, E. R.; Sun, L.; Hendon, C. H.; Walsh, A.; Van Voorhis, T.; Dincă, M. Cation-Dependent Intrinsic Electrical Conductivity in Isostructural Tetrathiafulvalene-Based Microporous Metal–Organic Frameworks. *J. Am. Chem. Soc.* **2015,** *137,* 1774–1777.
46. Sun, L.; Hendon, C. H.; Minier, M. A.; Walsh, A.; Dincă, M. Million-Fold Electrical Conductivity Enhancement in Fe_2(DEBDC) versus Mn_2(DEBDC) (E = S, O). *J. Am. Chem. Soc.* **2015,** *137,* 6164–6167.
47. Sheberla, D.; Sun, L.; Blood-Forsythe, M. A.; Er, S.; Wade, C. R.; Brozek, C. K.; Aspuru-Guzik, A.; Dincă, M. High Electrical Conductivity in Ni_3(2,3,6,7,10,11-hexaiminotriphenylene)$_2$, a Semiconducting Metal−Organic Graphene Analogue. *J. Am. Chem. Soc.* **2014,** *136,* 8859–8862.
48. Zeng, M.-H.; Wang, Q.-X.; Tan, Y.-X.; Hu, S.; Zhao, H.-X.; Long, L.-S.; Kurmoo, M. Rigid Pillars and Double Walls in a Porous Metal-Organic Framework: Single-Crystal to Single-Crystal, Controlled Uptake and Release of Iodine and Electrical Conductivity. *J. Am. Chem. Soc.* **2010,** *132,* 2561–2563.
49. Talin, A. A.; Centrone, A.; Ford, A. C.; Foster, M. E.; Stavila, V.; Haney, P.; Kinney, R. A.; Szalai, V.; Gabaly, F. E.; Yoon, H. P.; Léonard, F.; Allendorf, M. D. Tunable Electrical Conductivity in Metal-Organic Framework Thin-Film Devices. *Science* **2014,** *343,* 66–69.
50. Farnandez, C. A.; Martin, P. C.; Schaef, T.; Bowden, M. E.; Thallapally, P. K.; Dang, L.; Xu, W.; Chen, X.; McGrail, B. P. An Electrically Switchable Metal-Organic Framework. *Sci. Rep*. **2014,** *4,* 6114.
51. Guo, Z.; Panda, D. K.; Maity, K.; Lindsey, D.; Parker, T. G.; Albrecht-Schmitt, T. E.; Barreda-Esparza, J. L.; Xiong, P.; Zhou, W.; Saha, S. Modulating electrical conductivity of metal–organic framework films with intercalated guest π-systems. *J. Mater. Chem. C* **2016,** *4,* 894–899.

52. Guo, Z.; Panda, D. K.; Gordillo, M. A; Khatun, A.; Wu, H.; Zhou, W.; Saha, S. Lowering Band Gap of an Electroactive Metal–Organic Framework via Complementary Guest Intercalation. *ACS Appl. Mater. Interfaces* **2017,** *9,* 32413–32417.
53. Ramaswamy, P.; Wong, N. E.; Shimizu, G. K. H. MOFs as Proton Conductors — Challenges and Opportunities. *Chem. Soc. Rev.* **2014,** *43,* 5913–5932.
54. Horike, S.; Umeyama, D.; Kitagawa, S. Ion Conductivity and Transport by Porous Coordination Polymers and Metal-Organic Frameworks. *Acc. Chem. Res.* **2013,** *46*, 2376–2384.
55. Yoon, M.; Suh, K.; Natarajan, S.; Kim, K. Proton Conduction in Metal-Organic Frameworks and Related Modularly Built Porous Solids. *Angew. Chem. Int. Ed.* **2013,** *52*, 2688–2700.
56. Jeong, N. C.; Samanta, B.; Lee, C. Y.; Farha, O. K.; Hupp, J. T. Coordination-Chemistry Control of Proton Conductivity in the Ionic Metal–Organic Framework Material HKUST-1. *J. Am. Chem. Soc.* **2012,** *134,* 51–54.
57. Ameloot, R.; Aubrey, M.; Wiers, B. M.; Gómora-Figueroa, A. P.; Patel, S. N.; Balsara, N. P.; Long, J. R. Ionic Conductivity in the Metal-Organic Framework UiO-66 by Dehydration and Insertion of Lithium tert-Butoxide. *Chem. Eur. J.* **2013,** *19,* 5533–5536.
58. Cepeda, J.; Pérez-Yáñez, S.; Beobide, G.; Castillo, O.; Goikolea, E.; Aguesse, F.; Garrido, L.; Luque, A.; Wright, P. A. Scandium/Alkaline Metal-Organic Frameworks: Adsorptive Properties and Ionic Conductivity. *Chem. Mater.* **2016,** *28,* 2519–2528.
59. Fujie, K.; Ikeda, R.; Otsubo, K.; Yamada, T.; Kitagawa, H. Lithium Ion Diffusion in a Metal-Organic Framework Mediated by an Ionic Liquid. *Chem. Mater*. **2015,** *27,* 7355–7361.
60. Park, S. S.; Tulchinsky, Y.; Dincă, M. Single-Ion Li^+, Na^+, and Mg^{2+} Solid Electrolytes Supported by a Mesoporous Anionic Cu–Azolate Metal–Organic Framework. *J. Am. Chem. Soc.* **2017,** *139,* 13260–13263.
61. Panda, D. K.; Maity, K.; Palukoshka, A.; Ibrahim, F.; Saha, S. Li^+ Ion-Conducting Sulfonate-Based Neutral Metal–Organic Framework. *ACS Sus. Chem. Eng.* **2019,** *7,* 4619–4624.
62. Miner, E. M.; Park, S. S.; Dincă, M. High Li^+ and Mg^{2+} Conductivity in a Cu-Azolate Metal–Organic Framework. *J. Am. Chem. Soc.* **2019,** *141,* 4422–4427.
63. Lopez, H. A.; Dhakshinamoorthy, A.; Ferrer, B.; Atienzar, P.; Alvaro, M.; Garcia, H. Photochemical Response of Commercial MOFs: $Al_2(BDC)_3$ and Its Use as Active Material in Photovoltaic Devices. *J. Phys. Chem. C* **2011,** *115,* 22200–22206.
64. Lee, D. Y.; Kim, E.-K.; Shin, C. Y.; Shinde, D. V.; Lee, W.; Shrestha, N. K.; Lee, J. K.; Han, S.-H. Layer-by-Layer Deposition and Photovoltaic Property of Ru-based Metal–Organic Frameworks. *RSC Adv.* **2014,** *4,* 12037–12042.
65. Liu, J.; Zhou, W.; Liu, J.; Howard, I.; Kilibarda, G.; Schlabach, S.; Coupry, D.; Addicoat, M.; Yoneda, S.; Tsutsui, Y.; Sakurai, T.; Seki, S.; Wang, Z.; Lindemann, P.; Redel, E.; Heine, T.; Wöll, C. Photoinduced Charge-Carrier Generation in Epitaxial MOF Thin Films: High Efficiency as a Result of an Indirect Electronic Band Gap? *Angew. Chem. Int. Ed.* **2015,** *54,* 7441–7445.
66. Liu, J.; Zhou, W.; Liu, J.; Fujimori, Y.; Higashino, T.; Imahori, H.; Jiang, X.; Zhao, J.; Sakurai, T.; Hattaori, Y.; Matsuda, W.; Seki, S.; Garlapati, S. K.; Dasgupta, S.; Redel, E.; Sun, L.; Wöll, C. A New Class of Epitaxial Porphyrin Metal–Organic Framework Thin-Films with Extremely High Photocarrier Generation Efficiency: Promising Materials for All Solid-State Solar Cells. *J. Mater. Chem. A* **2016,** *4,* 12739–12747.

67. Maza, W.A.; Haring, A. J.; Ahrenholtz, S. R.; Epley, C. C.; Lin, S. Y.; Morris, A. J. Ruthenium(II)-Polypyridyl Zirconium(IV) Metal–Organic Frameworks As a New Class of Sensitized Solar Cells. *Chem. Sci.* **2016,** *7,* 719–727.

68. Goswami, S.; Ma, L.; Martinson, A. B. F.; Wasielewski, M. R.; Farha, O. K.; Hupp, J. T. Toward Metal–Organic Framework-Based Solar Cells: Enhancing Directional Exciton Transport by Collapsing Three-Dimensional Film Structures. *ACS Appl. Mater. Interfaces* **2016,** *8,* 30863–30870.

69. Spoerke, E. D.; Small, L. J.; Foster, M. E.; Wheeler, J.; Ullman, A. M.; Stavila, V.; Rodriguez, M.; Allendorf, M. D. MOF-Sensitized Solar Cells Enabled by a Pillared Porphyrin. *J. Phys. Chem. C* **2017,** *121,* 4816–4824.
70. Gordillo, M. A.; Panda, D. K.; Saha, S. Efficient MOF-Sensitized Solar Cells Featuring Solvothermally Grown [100]-Oriented Pillared Porphyrin Framework-11 Films on ZnO/FTO Surfaces. *ACS Appl. Mater. Interfaces* **2019,** *11,* 3196–3206.
71. Cui, Y.; Yue, Y.; Qian, G.; Chen, B. Luminescent functional metal–organic frameworks. *Chem. Rev.* **2012,** *112,* 1126–1162.
72. Lee, C. Y.; Farha, O. K.; Hong, B. J.; Sarjeant, A. A.; Nguyen, S. T.; Hupp, J. T. Light-Harvesting Metal-Organic Frameworks (MOFs): Efficient Strut-to-Strut Energy Transfer in Bodipy and Porphyrin-Based MOFs. *J. Am. Chem. Soc.* **2011,** *133,* 15858–15861.
73. Son, H.-J.; Jin, S.; Patwardhan, S.; Wezenberg, S. J.; Jeong, N. C.; So, M.; Wilmer, C. E.; Sarjeant, A. A.; Schatz, G. C.; Snurr, R. Q.; Farha, O. K.; Wiederrecht, G. P.; Hupp, J. T. Light-Harvesting and Ultrafast Energy Migration in Porphyrin-Based Metal-Organic Frameworks. *J. Am. Chem. Soc.* **2013,** *135,* 862–869.
74. Dolgopolova, E. A.; Rice, A. M.; Martin, C. R.; Shustova, N.B. Photochemistry and photophysics of MOFs: steps towards MOF-based sensing enhancements. *Chem. Soc. Rev.* **2018,** *47,* 4710–4728.
75. So, M. C.; Weiderrecht, G. P.; Mondloch, J. E.; Hupp, J. T.; Farha, O. K. Metal–organic framework materials for light-harvesting and energy transfer. *Chem. Commun.* **2015,** *51,* 3501–3510.
76. Williams, D. E.; Shustova, N. B. Metal-Organic Frameworks as a Versatile Tool to Study and Model Energy Transfer Processes. *Chem. Eur. J.* **2015,** *21,* 15474–15479.
77. Williams, D. E.; Rietman, J. A.; Maier, J. M.; Tan, R.; Greytak, A. B.; Smith, M. D.; Krause, J. A.; Shustova, N. B. Energy Transfer on Demand: Photoswitch-Directed Behavior of Metal-Porphyrin Frameworks. *J. Am. Chem. Soc.* **2014,** *136,* 11886–11889.
78. Dolgopolova, E. A.; Williams, D. E.; Greytak, A. B.; Rice, A. M.; Smith, M. D.; Krause, J. A.; Shustova, N. B. A Bio-inspired Approach for Chromophore Communication: Ligand-to-Ligand and Host-to-Guest Energy Transfer in Hybrid Crystalline Scaffolds. *Angew. Chem. Int. Ed.* **2015,** *54,* 13639–13643.
79. Zhang, Q.; Zhang, C.; Cao, L.; Wang, Z.; An, B.; Lin, Z.; Huang, R.; Zhang, Z.; Wang, C.; Lin, W. Förster Energy Transport in Metal–Organic Frameworks is beyond Step-by-Step Hopping. *J. Am. Chem. Soc.* **2016,** *138,* 5308–5315.
80. Maza, W. A.; Padilla, R.; Morris, A. J. Concentration Dependent Dimensionality of Resonance Energy Transfer in a Postsynthetically Doped Morphologically Homologous Analogue of UiO-67 MOF with Ruthenium (II) Polypyridyl Complex. *J. Am. Chem. Soc.* **2015,** *137,* 8161–8168.
81. Woodward, A. N.; Kolesar, J. M.; Hall, S. R.; Saleh, N.-A.; Jones, D. S.; Walter, M. G. Thiazolothiazole Fluorophores Exhibiting Strong Fluorescence and Viologen-Like Reversible Electrochromism. *J. Am. Chem. Soc.* **2017,** *139,* 8467−8473.

82. Roy, I.; Bobbla, S.; Zhou, J.; Nguyen, M. T.; Nalluri, S. K. M.; Wu, Y.; Ferris, D. P.; Scott, A. E.; Wasielewski, M. R.; Stoddart, J. F. ExTzBox: A Glowing Cyclophane for Live-Cell Imaging. *J. Am. Chem. Soc.* **2018,** *140,* 7206–7212.
83. Rizzuto, F. J.; Faust, T. B.; Chan, B.; Hua, C.; D'Alessandro, D. M.; Kepert, C. J. Experimental and Computational Studies of a Multi-Electron Donor-Acceptor Ligand Containing the Thiazolo[5,4-*d*]thiazole Core and its Incorporation into a Metal–Organic Framework. *Chem. Eur. J.* **2014,** *20,* 17597–17605.
84. Millan, S.; Makhloufi, G.; Janiak, C. Incorporating the Thiazolo[5,4-*d*]thiazole Unit into a Corrdination Polymer with Interdigitated Structure. *Crystals* **2018,** *8,* 30:1–13.
85. Zhai, Z.-W.; Yang, S.-H.; Cao, M.; Li, L.-K.; Du, C.-X.; Zang, S-Q. Rational Design of Three Two-Fold Interpenetrated Metal−Organic Frameworks: Luminescent Zn/Cd-Metal−Organic Frameworks for Detection of 2,4,6-Trinitrophenol and Nitrofurazone in the Aqueous Phase. *Cryst. Growth. Des.* **2018**, *18*, 7173–7182.
86. Hisamatsu, S.; Masu, H.; Azumaya, I.; Takahashi, M.; Kishikawa, K; Kohmoto, S. U-Shaped Aromatic Ureadicarboxylic Acids as Versatile Building Blocks: Construction of Ladder and Zigzag Networks and Channels. *Cryst. Growth Des*. **2011,** *11,* 5387–5395.
87. Ma, B.-Q., Mulfort, K. L.; Hupp, J. T. Microporous pillared paddle-wheel based on mixed-ligand coordination of zinc ions. *Inorg. Chem.* **2005,** *44,* 4912–4914.
88. Chun, H.; Dybtsev, D. N.; Kim, H.; Kim, K. Synthesis, X-ray Crystal Structures, and Gas Sorption Properties of Pillared Square Grid Nets Based on Paddle-Wheel Motifs: Implications for Hydrogen Storage in Porous Materials. *Chem. Eur. J*. **2005,** *11,* 3521–3529.
89. Berlman, I. B.; Weinreb, A. On the fluorescence spectrum and decay time of naphthalene. *Mol. Phys.* **1962,** *5,* 313–319.
90. Sun, Q.; Aguila, B.; Perman, J.; Earl, L.; Abney, C.; Cheng, Y.; Wei, H.; Nguyen, N.; Wojtas, L.; Ma, S. Post-synthetically Modified Covalent Organic Frameworks for Efficient and Effective Mercury Removal. *J. Am. Chem. Soc.* **2017**, *139*, 2786–2793.
91. Aguila, B.; Sun, Q.; Perman, J. A.; Earl, L. D.; Abney, C. W.; Elzein, R.; Schlaf, R.; Ma, S. Efficient Mercury Capture Using Functionalized Porous Organic Polymer. *Adv. Mater.* **2017,** *29,* 1700665.
92. Li, B.; Zhang, Y.; Ma, D.; Shi, Z.; Ma, S. Mercury Nano-Trap for Effective and Efficient Removal of Mercury(II) from Aqueous Solution. *Nat. Commun.* **2014,** *5,* 5537.
93. Lalonde, M.; Bury, W.; Karagiaridi, O.; Brown, Z.; Hupp, J. T.; Farha, O. M. Transmetalation: routes to metal exchange within metal–organic frameworks. *J. Mater. Chem. A,* **2013,** *1,* 5453–5468.

For Table of Contents Only

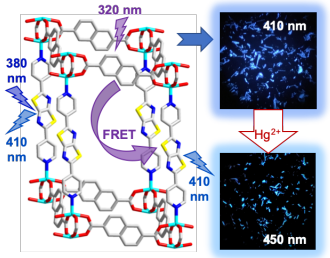

A new blue-light emitting pillared-paddlewheel metal–organic framework featuring energy donating naphthalene dicarboxylate struts and energy accepting thiazolothiazole pillars displays ligand-to-ligand energy transfer and Hg(II) ion-induced bathochromic fluorescence shift.